Structural hierarchy in blends of amphiphilic block copolymers self-assembled at the air-water interface

Janet Hood, Kyle Van Gordon, Patricia Thomson, Brian R. Coleman, Fraser Burns, & Matthew G. Moffitt

November 2019

The final publication is available at:

https://doi.org/10.1016/j.jcis.2019.08.080

Structural Hierarchy in Blends of Amphiphilic Block Copolymers Self-Assembled at the Air-Water Interface

Janet Hood, Kyle Van Gordon, Patricia Thomson, Brian R. Coleman, Fraser Burns, and Matthew G. Moffitt*

Department of Chemistry, University of Victoria, PO Box 1700 Stn CSC, Victoria BC V8W 2Y2 Canada

Abstract

We present a concurrent self-assembly strategy for patterning hierarchical polymeric surface features by depositing variable-composition blends of polystyrene-*block*-poly(ethylene oxide) (PS-*b*-PEO) and polybutadiene-*block*-poly(ethylene oxide) (PB-*b*-PEO) block copolymers at the air-water interface. Hierarchical strand networks of hydrophobic PS/PB blocks anchored *via* PEO blocks to the water surface, with an internal phase-separation structure consisting of periodic domains of PS blocks surrounded and connected by a matrix of PB blocks, are generated by the interplay of interfacial amphiphilic block copolymer aggregation and polymer/polymer phase separation. In contrast to the cylinder-in-strand structures previously formed by our group in which interfacial microphase separation between PS and PB blocks was constrained by chemical connectivity between the blocks, in the current system phase separation between PS and PB is not constrained by chemical connectivity and yet is confined laterally within surface features at the air-water interface. Investigations of multi-component polymer systems with different connectivities constraining repulsive and attractive interactions provides routes to new hierarchical surface patterns for a variety of applications, including photolithography masks, display technology, surface-guided cell growth and tissue engineering.

TOC Graphic

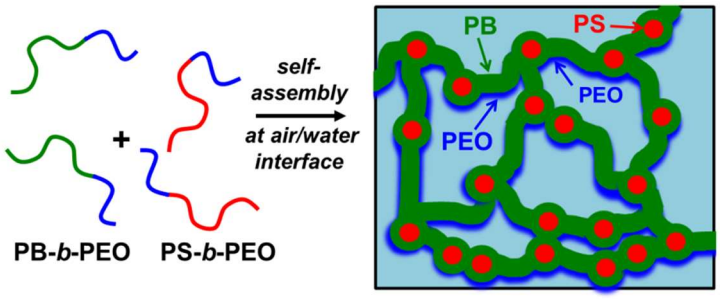

Keywords: Langmuir-Blodgett films; block copolymers; blends; self-assembly; patterning; nanostructures; polymer films

Introduction

Molecular self-assembly provides efficient pathways to materials with tunable function arising from complex structure on multiple length scales. A facile and versatile strategy for achieving spontaneous structural hierarchy is the concurrent self-assembly of two or more different building blocks through a combination of competitive and cooperative structure-forming processes on different length scales.[1] For example, various combinations of surfactants,[2] phospholipids,[3,4] block copolymers,[5-7] and nanoparticles[8-11] have been shown to undergo multiscale organization in organic and aqueous solvent environments through a complex interplay of repulsive and attractive interactions, giving rise to a wide range of three-dimensional (3D) mesoscale colloids with nanoscale surface patterns or internal compartments.

The two-dimensional (2D) self-assembly of block copolymer amphiphiles at the air-water interface has been widely studied since 2D micelle formation was first reported by Zhu et al. in 1991.[12] In these systems, the block copolymer molecules are first dissolved in a common solvent for both blocks, and then deposited on the water surface of a film balance to generate a Langmuir film.[13-24] Spreading and solvent evaporation gives rise to aggregation of the hydrophobic blocks into various surface structures, including dots, strands, continents, chains, and rings, depending on the block copolymer composition and spreading concentration. The resulting aggregate morphologies, which can be transferred to solid substrates using Langmuir-Blodgett (LB) techniques, are influenced by a combination of thermodynamic forces, including attractive/repulsive interactions between the hydrophilic/hydrophobic blocks and the water surface,[14,15] and kinetic factors, including chain entanglements and polymer vitrification.[17-19,21,22]

In addition to Langmuir films consisting of a single amphiphilic block copolymer component, a variety of hierarchical surface structures have been generated *via* concurrent self-

assembly of multiple components at the air-water interface. For example, 2D polymer-nanoparticle composite surface features have been formed from blends of hydrophobic inorganic nanoparticles and amphiphilic block copolymers spread at the water surface,[25,26] including mesoscale polymeric strands with internal dispersions of nanoscale quantum dots.[27,28] In other work, our group reported cylinder-in-strand features formed at the air-water interface *via* concurrent self-assembly of the amphiphilic block copolymer polystyrene-*block*-poly(ethylene oxide) (PS-*b*-PEO) and the hydrophobic block copolymer polystyrene-*block*-polybutadiene (PS-*b*-PB); spreading and solvent evaporation gave way to aggregation of various hydrophobic blocks to generate mesoscale strands, while microphase separation between covalently-connected PS and PB blocks within each strand resulted in an internal structure of nanoscale cylinders.[29]

Investigating the self-assembly of multi-component polymer systems with *different* connectivities in interfacial environments introduces *different* constraints to repulsive and attractive interactions, providing new routes to hierarchical surface patterns for a variety of applications, including photolithography masks, display technology, surface-guided cell growth and tissue engineering. For example, a central pillar of soft nanomaterials research is the microphase separation between the covalently connected and chemically dissimilar blocks of block copolymers to generate ordered patterns of nanoscale dimensions.[30] A related process on much longer length scales is the phase separation of non-connected and dissimilar polymer chains *via* spinodal decomposition within polymer blends, which forms microscale and macroscale domain patterns.[31] In order to direct pattern formation in both of these phase separation processes, many groups have explored the use of solid surfaces to introduce physical and chemical confinement.[32-37] However, an interesting and completely novel idea is to investigate polymer-polymer phase separation confined to a liquid surface, by separately anchoring the dissimilar phase-separating

blocks to the air-water interface *via* attached hydrophilic blocks. Unlike solid surfaces, the air-liquid interface is dynamic, providing both unique variability and transferability of the resulting patterns. Although there have been a few studies on the phase separation of non-connected homopolymers at the air-water interface,[38-40] to our knowledge none of these studies have applied the unique lateral confinement to phase separation which should arise from anchoring the dissimilar chains to the water surface.

In this paper, we investigate the concurrent self-assembly of PS-*b*-PEO and PB-*b*-PEO at the air-water interface, comparing Langmuir monolayers and transferred LB films of the individual and blended components. The blend system represents an interesting case of interfacial co-assembly of amphiphilic block copolymers with similar hydrophilic blocks but different and incompatible hydrophobic blocks. The resulting tandem interactions of net repulsion between hydrophobic blocks and the water surface and net repulsion between hydrophobic blocks on different amphiphiles leads to phase separation between PS and PB that is not constrained by chemical connectivity and yet is confined laterally within surface features arising from aggregate formation at the air-water interface. We note that these tandem processes and the resulting aggregates are completely distinct from the cylinder-in-strand structures we have reported in ref. 29,[29] since in that previous work phase separation between PS and PB blocks was constrained by chemical connectivity between the blocks, leading to nanoscale cylinders governed by thermodynamics. In contrast, in the current work, phase separation between PS and PB blocks is not constrained by chemical connectivity but instead is confined to the liquid surface within kinetically-determined surface aggregates,[18,19] leading to very different phase domains structures. To our knowledge, such an example of concurrent self-assembly of incompatible block copolymer amphiphiles in Langmuir films has not been previously reported. We report interesting periodic

hierarchical surface features generated from blends of PS-*b*-PEO and PB-*b*-PEO, consisting of networks of PB strands connecting and surrounding internal PS domains (Figure 1).

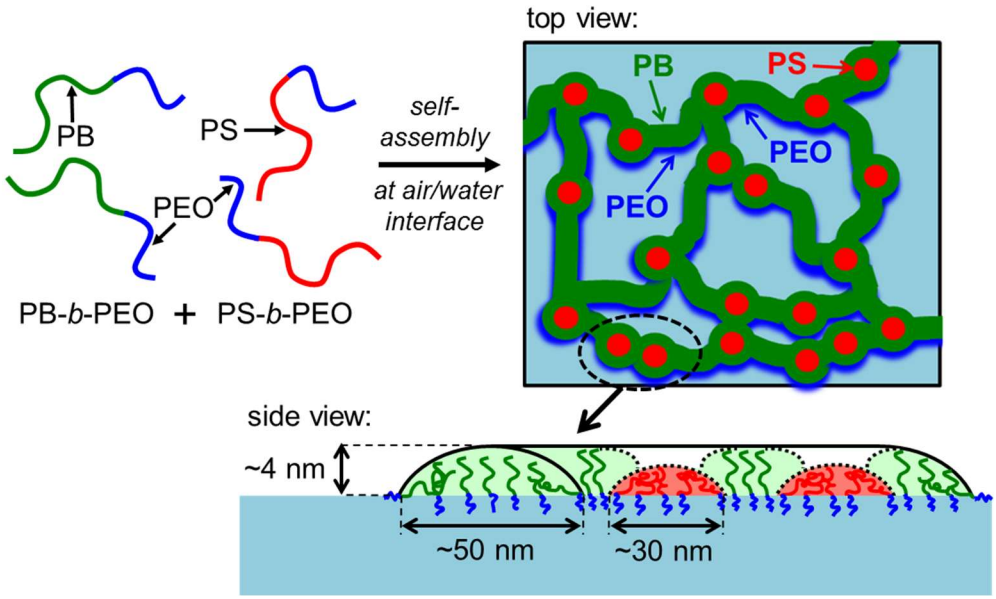

Figure 1. Schematic showing concurrent self-assembly of PS-*b*-PEO and PB-*b*-PEO at the air-water interface and the resulting hierarchical assemblies. The proposed structure and reported dimensions were determined based on a combination of TEM and AFM images as described in the text.

Experimental

Materials. Three diblock copolymers were used in this study: a polystyrene-*block*-poly(ethylene oxide) copolymer (SEO: M_n= 148k; 12.2 wt % PEO; M_w / M_n = 1.09) and two similar polybutadiene-*block*-poly(ethylene oxide) copolymers (BEO1: M_n = 71k; 14.1 wt. % PEO; M_w / M_n = 1.05 and BEO2: M_n = 76k; 21.1 wt. % PEO; M_w / M_n = 1.10) were purchased from Polymer Source Inc. and used without further purification. Initial isotherm and LB experiments were carried out using the BEO1 copolymer; due to sample limitation, subsequent follow-up experiments were carried out using the BEO2 copolymer. BEO1 and BEO2 have very similar PB

block lengths ($M_{n,PB}$ = 61k and 60k for BEO1 and BEO2, respectively), but the PEO block length of BEO1 ($M_{n,PEO}$ = 10k) is slightly shorter than that of BEO2 ($M_{n,PEO}$ = 16k). As discussed in the main text, we found qualitatively similar time-dependent isotherm behaviour for both BEO1 and BEO2, suggesting that the described experiments using BEO2 complement and shed light on the results of experiments using BEO1.

Preparation of Polymer Solutions. Polymers were dried in a vacuum oven overnight to ensure they were free of water prior to solution preparation. All solutions were prepared in glass vials that had been rinsed three times with filtered chloroform. Stock solutions of SEO and BEO block copolymers at 5.0 mg/mL were prepared using filtered spectroscopic grade chloroform (99.8% Caledon). Stock solutions were stirred for ~4 h after solvent addition and then left to equilibrate overnight. After equilibration, the SEO and BEO stock solutions were either diluted individually with filtered chloroform to 2.0 mg/mL, or else various relative amounts of SEO and BEO stock solutions were mixed and then diluted with filtered chloroform to 2.0 mg/mL to form SEO/BEO blend solutions of various BEO weight fractions (relative to the total polymer content), f_{BEO}; all solutions (SEO, BEO, and SEO/BEO) were stirred for ~1 h after dilution. Solutions were stored in the freezer in sealed vials covered in aluminum foil when not in use and were used within 7 days. After removal from the freezer, solutions were allowed to equilibrate to room temperature prior to isotherm or Langmuir-Blodgett experiments.

Surface Pressure – Area Isotherms of Langmuir Films. Surface pressure-area isotherms and LB films were obtained using a KSV 3000 Langmuir trough (KSV Instruments Ltd.) secured inside a dust shield. The total trough surface area was 150 x 515 mm^2 and the total trough volume was ~1L. The tough area was robotically controlled by two hydrophobic paddles, which compressed the spread film symmetrically and bilaterally at a rate of 10 mm/min. House-distilled

deionized water (Barnstead NANOpure Diamond, 18.2 mΩ·cm) was used as the subphase in all trials. For all experiments, the subphase temperature was controlled at 25 ± 1 ºC. Prior to filling the trough with the subphase, the LB components were cleaned 3x with ethanol and 3x with deionized water. Prior to solution deposition, the water surface was cleaned by aspirating off any debris such that the surface pressure remained < 0.20 mN/m over a full compression. Surface pressure measurements were made from a roughened platinum Wilhemy plate which was flamed for 10 s prior to each trial to ensure cleanliness.

For all isotherm experiments, an appropriate volume of 2.0 mg/mL solution was deposited on the subphase from a gastight Hamilton syringe, in order to deposit 0.025 mg total polymer solid (12.5 μL solution) on the water surface. The spreading solution was deposited dropwise at regularly spaced locations on the trough. After 30 min evaporation/spreading time, the film was compressed at a rate of 10 mm/min to the limits of the trough. Monitoring π, defined as the difference between the surface tension of pure water and that of the deposited film ($\pi = \gamma_0 - \gamma$), as a function of total trough area A resulted in the $\pi - A$ isotherm.

Langmuir-Blodgett Film Preparation. Glass substrates (Fisher Scientific, 18 mm x 18 mm) for Langmuir-Blodgett (LB) experiments were cleaned by first sonicating in methanol for 20 min, then sonicating in spectroscopic grade chloroform for 20 min. TEM substrates were prepared in the following manner: Cu grids (SPM Labs, 300 mesh) were fixed onto glass first by floating a thin film of Formvar over a deionized water subphase, transferring 3 or 4 Cu TEM grids to the floating Formvar film, and then scooping the grid/Formvar film onto a clean glass substrate so that the grids were sandwiched between the Formvar and glass. After drying overnight in a petri dish, a thin layer of carbon was evaporated onto the Formvar to generate carbon/Formvar-coated Cu grids. LB film transfer experiments were conducted by submerging the glass substrate with

attached TEM grids and a clean glass slide (for AFM imaging) held in tandem on a modified dipper head with binder clips prior to depositing the copolymer solution. For all LB experiments, 0.025 mg total solid polymer (12.5 μL solution) was deposited on the subphase from a gastight Hamilton syringe, in an identical manner to solution deposition for isotherm experiments; after 30 min evaporation/spreading, the film was compressed to a surface pressure of π = 12 mN/m (unless otherwise noted) and held for another 30 min. The submerged substrates were then raised through the air-water interface at a rate of 1 mm/min to obtain transfer ratios of 0.7-1.2 for all imaged LB films with the following exceptions: pure BEO1 and the SEO/BEO2 (f_{BEO} = 0.75) blend had a transfer ratios of 0.5 and 1.9, respectively. All transferred LB films were dried vertically for a minimum of 12 h before imaging.

Transmission Electron Microscopy. TEM was performed on a JEOL JEM-1400 electron microscope operating at an accelerating voltage of 80 kV and equipped with a Gatan Orius SC1000 CCD camera. The SEO/BEO blend LB films on carbon/Formvar-coated Cu grids were stained with the vapors of 4% aqueous osmium tetraoxide (OsO_4) solution for ~3 h before imaging. This processes provided selective staining for PB-rich domains and minimal staining of PS-rich domains. The SEO LB films were imaged without staining.

Atomic Force Microscopy. AFM was performed on a Veeco (ThermoMicroscopes Explorer) Instrument equipped with a 190 kHz uncoated silicon cantilever probe (Ted Pella Inc.) operating in tapping mode. The sample assembly was housed in a glass shield and the entire microscope was located on an isolation platform (80 psi) to reduce vibration on the oscilloscope.

Results and Discussion

Isotherms. Representative π-A compression isotherms for SEO and BEO1 copolymers and the SEO/BEO1 (f_{BEO} = 0.50) blend at the air-water interface are shown in Figure 2. For better comparison of the three deposited samples with different average molecular weights, the isotherms are represented using total trough area rather than mean molecular area.

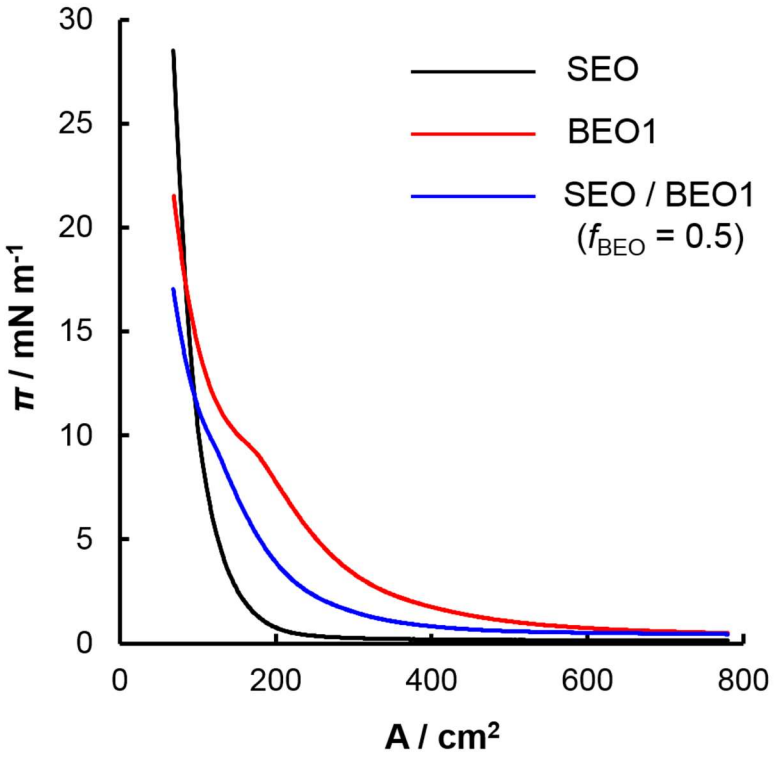

Figure 2. Langmuir compression isotherms of SEO (black), BEO1 (red), and SEO/BEO1 (f_{BEO} = 0.50) blend (blue).

The SEO isotherm shows a steep and featureless increase in π, starting at A = ~200 cm^2, associated with the overlap of condensed and glassy PS blocks. The absence of a plateau or pseudo-plateau at π = ~10 mN/m, generally attributed to a phase transition induced by strong overlap of PEO blocks on the water surface,[13-19] suggests that most of the PEO chains are trapped underneath

the PS layer, as is often found in isotherms of PS-*b*-PEO with largely hydrophobic compositions.[17-19] The BEO1 isotherm shows an earlier and more gradual increase in π than the SEO isotherm, starting at A = ~600 cm^2, associated with the overlap of expanded and flexible PEO blocks on the water surface.[13-19] As the film is further compressed, an inflection, or pseudo-plateau in the isotherm occurs at π = ~10 mN/m, attributed to a phase transition of overlapping PEO chains,[13-19] followed by a steep upturn in surface pressure due to overlapping PB blocks. The isotherm of the SEO/BEO1 blend (blue curve) shows behaviour in between that of the pure components, with a slight inflection at π = ~10 mN/m (although less distinct than in the BEO1 case), and an onset of π increase (starting at A = ~400 cm^2) in between that of SEO and BEO1.

Comparison of the SEO and BEO1 compression isotherms indicates a stronger contribution from the PEO blocks in the BEO1 case, despite the PEO blocks being significantly longer in the SEO copolymer (18k compared to 10k). This is evidenced both by the earlier upturn in π and the pseudo-plateau at π = ~10 mN/m in the BEO1 case. Both of these features are attributed to overlapping PEO chains as described in the previous literature,[13-19] including comparisons of isotherm behaviour of pure PEO with PEO-based copolymers containing hydrophobic blocks of variable length.[14] It has also been shown that relatively large hydrophobic block fractions can hinder the overlap of PEO blocks upon compression due to a combination of steric interactions between PS aggregates and repulsive interactions between PS and PEO chains, leading to a later and steeper upturn in π and the absence of a pseudo-plateau.[14,15,17-19] Therefore one contribution to the difference in the compression isotherms may be the somewhat higher PEO weight fraction in the BEO1 case (14.1 wt %) compared to the SEO case (12.2 wt %). In addition, the different properties of PS and PB blocks may play a role in the different interfacial behaviours of SEO and BEO1. Specifically, despite the general thermodynamic favourability of PEO adsorption at the

water surface,[14-16] PS vitrification and kinetic trapping of hydrophobic blocks is expected to impede PEO adsorption in the SEO case, but not in the BEO1 case where the hydrophobic blocks are significantly above their glass transition temperature, even after solvent evaporation. As discussed previously in the literature[13-19] fast solvent evaporation can lead to a significant portion of PEO chains being trapped underneath the PS layer in SEO Langmuir films, especially in cases of largely hydrophobic copolymers at high spreading concentrations.[17-19]

Structural Hierarchy in PS-*b*-PEO / PB-*b*-PEO Langmuir-Blodgett Films. Next, we investigated the structure of transferred LB films of the SEO/BEO1 (f_{BEO} = 0.50) blend and its pure constituents. For all LB film preparations, solution volumes of 12.5 μL containing total solid amounts of 0.025 mg SEO, BEO1, or SEO/BEO1 were deposited at the air-water interface. The solutions were allowed to spread and evaporate for 30 min before compression then transferred to solid substrates at constant surface pressure. TEM and/or AFM imaging of LB films of block copolymer surface aggregates transferred from the water surface to solid substrates is a common although indirect method of obtaining information on the structure of aggregates as they existed at the air-water interface prior to transfer.[12,16-22] This method requires that the aggregates maintain their basic structural integrity upon compression and transfer, which has been demonstrated for PS-*b*-PEO aggregates due to vitrification of PS blocks upon solvent evaporation.[16] In the resulting LB films, aggregates of hydrophobic blocks appear raised by AFM or dark by TEM relative to the solid substrate, while the hydrophilic blocks form a thin layer at the substrate underneath and surrounding the aggregates and are generally not visible by either imaging technique.[12,16-22]

Due to the above considerations, our attempts to image LB films of pure BEO1 copolymer were unsuccessful at both investigated surface pressures (π = 2 and 5 mN/m), as no PB aggregates could be found on TEM grids of the transferred films, despite TR values between 0.5 and ~1 (see

Supporting Information for sample TEM image of pure BEO1, Figure S1). LB films at the reported surface pressures were selected for imaging as these gave the best TR values. TR values close to unity suggest that the BEO1 copolymer was successfully transferred to the substrate under these conditions and that low surface coverage could not explain he featureless nature of the LB films. Therefore, further substrate cleaning or surface activation were not attempted. Rather, we attribute the absence of aggregates on the grids to the dynamic and viscoelastic nature of PB, such that aggregates present at the air-water interface do not retain their structural integrity during compression and transfer. In contrast, TEM imaging of the pure SEO LB film (Figure 3) reveal continents and strands typical of this copolymer composition and spreading concentration.[18,19] The continents with holes found in some regions of the grid (Figure 3A) provide evidence of the dewetting/film rupture mechanism discussed previously in the literature.[19,22]

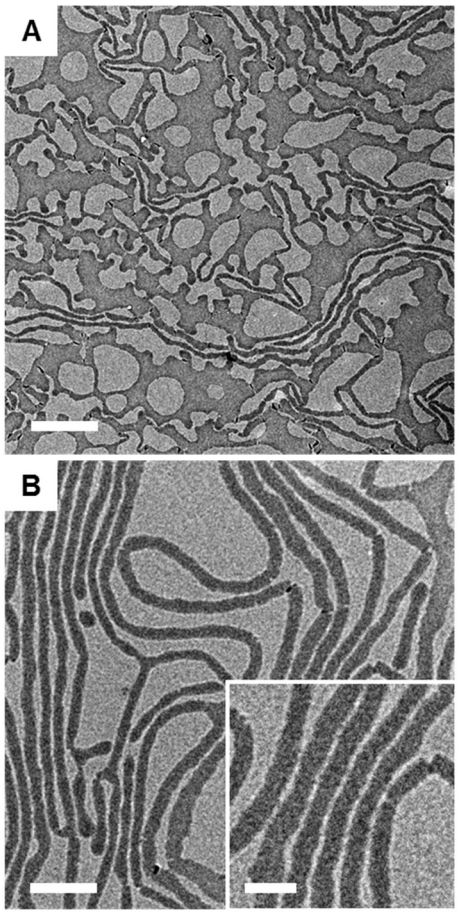

Figure 3. TEM of LB film of SEO at low (A), medium (B) and high (B, inset) magnification. The LB film was transferred at π = 12 mN/m. Scale bars represent 1 μm (A), 400 nm (B), and 200 nm (B, inset).

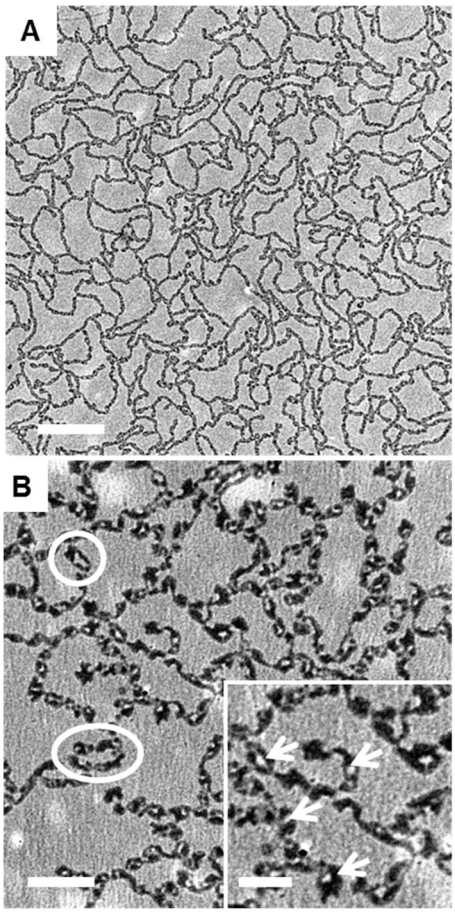

Figure 4. TEM of LB film of SEO/BEO1 (f_{BEO} = 0.50) blend at low (A), medium (B) and high (B, inset) magnification. The LB film was transferred at π = 12 mN/m. White circles in (B) highlight nodules or groups of nodules that have separated from the interconnected network; white arrows in (B, inset) highlight the light-contrast PS domains within the dark-contrast PB phase. Scale bars represent 1 μm (A), 400 nm (B), and 200 nm (B, inset).

TEM of the stained SEO/BEO1 (f_{BEO} = 0.50) LB film at low magnification (Figure 4A) shows interconnected strands similar to the LB film of pure SEO, with a mean strand width of ~50 nm. Higher magnification of the strands (Figure 4) reveals the hierarchical structure arising from concurrent self-assembly of the two blend components at the air-water interface. The selective staining of PB blocks by electron-dense OsO_4 provides chemical identification of PB- and PS-rich domains in TEM images, as previously shown in the literature.[41,42] The strands are seen to be an

interconnected network of nodules with the darker, more electron-dense domains (PB-rich, after OsO_4 staining) enveloping and connecting the nodules, with roughly-circular lighter domains (PS-rich) at the center of each nodule. The PS domains give rise to a periodic polymer composition profile along the strands. Several of the internal PS domains are identified with white arrows in the inset to Figure 4B. The nodular hierarchical structure results in irregularity in the widths of the interconnected strands, along with several regions where the individual nodules or strings of nodules appear to have separated from the connected network (Figure 4B, white circles).

Figure 1 summarizes the hierarchical structure of SEO/BEO1 (f_{BEO} = 0.50 LB) films, arising from the interplay of two simultaneous processes triggered by spreading and solvent evaporation. In the first process, aggregate formation is driven by the repulsion between both hydrophobic block types (PS and PB) and water, giving rise to blended PS/PB aggregates in the form of interconnected strands, similar to the interfacial aggregates formed from pure SEO (Figure 3). In the second process, phase separation of PS and PB blocks *within the strands* is driven by their mutual incompatibility as the spreading solvent evaporates; this process gives rise to the formation of internal PS and PB domains as the chemically-dissimilar hydrophobic components undergo phase segregation. Both the polymer-polymer phase separation[31] and surface aggregation[18,19] processes occur far from thermodynamic equilibrium and are arrested by fast solvent evaporation, giving rise to multiscale features that are kinetic rather than thermodynamic products. In this sense, the resulting patterns are very different from lipid monolayer structures arising from free-energy minimization at the air-water interface.[43] Rather, the network of strand-like aggregates are instead explained by kinetically trapped patterns arising from non-equilibrium de-wetting of hydrophobic blocks from the water surface, as described in previously,[19,22] although

in the present case the aggregates exhibit internal structure arising from confined PS-PB spinodal decomposition within the aggregates.

Unlike an earlier example of hierarchical LB films containing microphase-separated PS-*b*-PB block copolymer,[29] phase separation of PS and PB components in the present system is not restricted by covalent connectivity although it is confined laterally within the hydrophobic aggregates, giving rise to a polymer composition profile that is periodic in one dimension along the length of the strands. An important feature of the resulting structure is that, rather than alternating stripes of PS and PB along the strands, confined phase separation leads to circular domains of PS surrounded by external layers of PB distributed along the strands, with connections between nodules provided by pure PB. We attribute this aspect of the phase structure to the lower critical surface tension of the PB blocks compared to the PS blocks, which favors a wetting layer of the former component.[44] It is also noteworthy that, unlike the aggregates of pure BEO1 that are presumed to form at the water surface, the observed aggregates of SEO/BEO1 maintain structural integrity during LB transfer despite consisting of a soft PB matrix/external layer. Although some structural perturbations during LB transfer to the substrates cannot be ruled out, the general integrity of these aggregates is likely a result of the same cohesive energy between PB and PS phases that leads to the PB wetting layer, with the rigid internal PS phase acting as a skeleton or scaffold for the soft PB skin of the hierarchical strands.

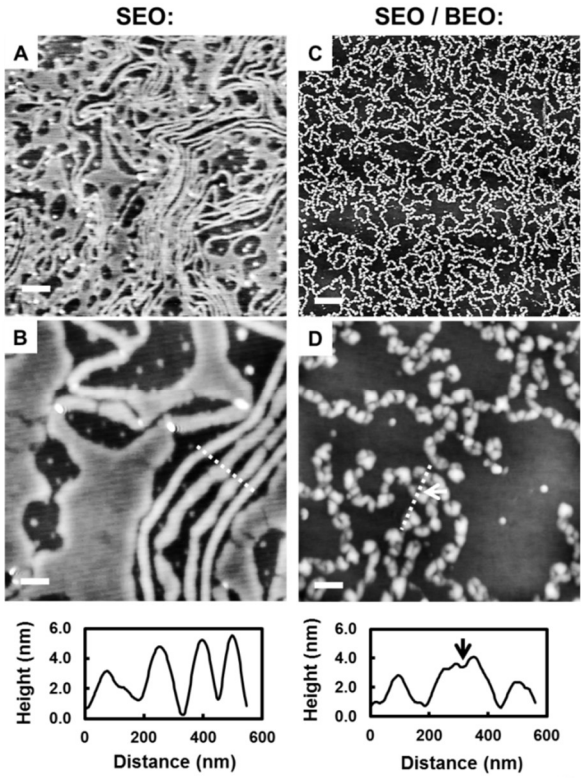

Figure 5. AFM of LB films of SEO (A and B) and SEO/BEO1 (f_{BEO} = 0.50) blend (C and D) transferred at a surface pressure of π = 12 mN/m. High magnification scans (B and D) include associated height profiles for features along the dotted white lines. White arrow in (D) indicates dark-contrast PS domain corresponding to height depression in the strand feature (black arrow in the corresponding height profile). Scale bars represent 1 μm (A and C) and 200 nm (B and D).

AFM imaging of LB films of SEO (Figure 5, A and B) and the SEO/BEO1 (f_{BEO} = 0.50) blend (Figure 5, C and D) transferred to glass substrates provides complementary topographical information on the respective surface aggregates. The lateral morphological information visible in the low magnification scans (Figure 5, A and C) is consistent with the TEM images of the equivalent films; this is expected since, unlike aggregates of pure BEO, SEO and SEO-containing blend aggregates will be kinetically frozen at the water surface following solvent evaporation such that the nature of the substrate will not affect the observed structures. The high magnification scan of the SEO film (Figure 5B) provides relative height information of the various features, with

lighter regions representing taller features on the grid. An additional finding is that strand aggregates are taller than continent aggregates, which are taller along their rims than in their central regions, consistent with previous results for SEO LB films.[17, 18, 19] From the height profile across the dotted line in Figure 5B, the strands are seen to be uniform in both width and height, with a strand height of ~5 nm determined from the profile. The high magnification scan of the SEO/BEO1 blend film (Figure 5D) show that the phase separation structures visible in TEM (Figure 4) correspond to different heights of internal structures within the strands. Specifically, the internal PS domains (light contrast in TEM, Figure 4B) appear as dark regions in AFM (Figure 5D), indicating that they are lower than the surrounding PB phase. This is clearly shown in the associated height profile (Figure 5D), for which the middle strand in the group traversed by the dotted line possesses a clear height depression where the line passes through the center of a nodule. The lower height level of the PS phase is attributed to PS having a higher critical surface tension (33.5 mN/m^2) compared to PB (28.5 mN/m), leading to a tendency of PB to wet PS domains in order to reduce the area of exposed PS.[45] As discussed previously, this tendency of PB to wet PS is also evident in the lateral phase structure observed by TEM, since PS domains are seen to be surrounded by a layer of PB in Figure 4B. However, as determined by complementary AFM data and as portrayed in the schematic in Figure 1, a complete layer of PB over the top of the PS domains is precluded by the anchoring of both components to the water surface *via* connected PEO blocks, giving rise to the observed depressions of PS within a pitted PB phase (Figure 5D).

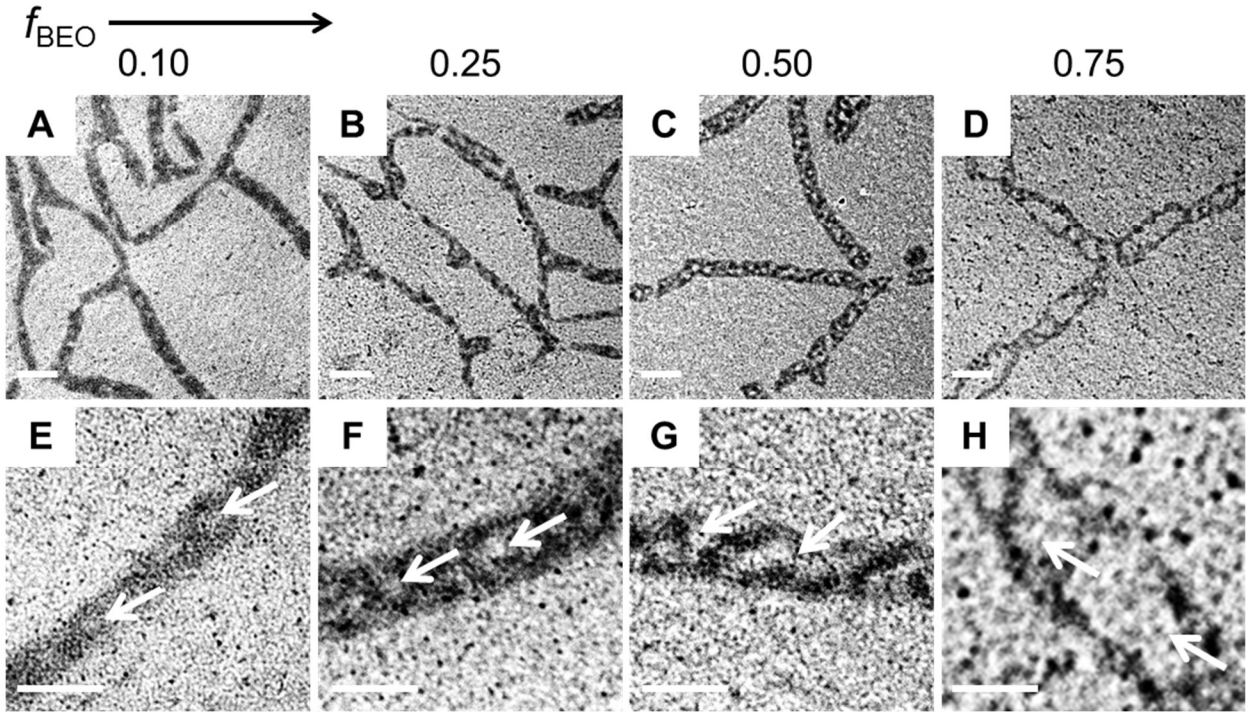

Figure 6. Effect of blend composition on phase-separation structure within LB films of SEO/BEO2. Low-magnification (A-D) and high-magnification (E-H) TEM images of SEO/BEO2 blends of various BEO weight fractions, f_{BEO}, transferred at a surface pressure of π = 5 mN/m. White arrows in high-magnification images indicate PS-rich domains. Scale bars are 200 nm and 100 nm for the low- and high-magnification images, respectively.

Finally, we explored the dependence of blend composition on the hierarchical structure of PS-*b*-PEO/PB-*b*-PEO LB films. For these experiments, PEO/BEO2 blends with four different BEO weight fractions, f_{BEO} = 0.10, 0.25, 0.50, and 0.75, were deposited at the air-water interface then the corresponding LB films were transferred at a surface pressure of π = 5 mN/m. Low-magnification TEM images in Figure 6 (A-D) show a similar structure of interconnected strands for all compositions, although the internal structures of the strands are markedly different. In the corresponding high-magnification TEM images (Figure 6, E-H), it is apparent that bright PS-rich domains (white arrows) become larger and more distinct as f_{BEO} increases. This trend can be

understood in terms of the difference in chain dynamics in the mixed state of the blends as the last of the solvent evaporates. When f_{BEO} is low (e.g. f_{BEO} = 0.10, Figure 6E), the hydrophobic strands consist mainly of high-T_g PS chains, leading to early vitrification of the strands such that the development of internal phase structure is kinetically impeded and the resulting PS-rich domains are small (~20 nm) and indistinct. As the f_{BEO} content increases, the mixed state of the strands will consist of an increasing percentage of low-T_g PB chains, providing faster chain dynamics and allowing more extensive development of phase structure in the final stages of solvent evaporation. For example when f_{BEO} = 0.75, the resulting LB films show an internal structure of distinct, ~100 nm-wide PS domains each surrounded by a ~25 nm-thick wall of PB distributed along the strands. We note that the larger areal contribution of PS within the strands of the f_{BEO} = 0.75 blend indicates a significantly higher chain density within the PB domains. The results of Figure 6 suggest that blend composition provides a useful kinetic handle through which the internal structure of these hierarchical strands can be tuned.

Another observation is that although the contrast between light PS and dark PB domains in Figure 6 allows the phase structure to be resolved, the contrast between the PS domains and carbon background is weaker in this series of images than in Figure 4, where the PS domains appear as clear white spots. This may be due to the slightly different BEO samples used in these two experiments or to different thicknesses of the carbon substrate. Such contrast limitations may be mitigated in future studies by characterization tools such as phase contrast AFM.

Due to the different surface energies of PB and PS blocks, we considered the possibility of preferential transfer of SEO and BEO copolymers to the solid substrates from floating films of the copolymer blends. Such preferential transfer does not appear to be a likely scenario, since transfer ratios of the blend films of various compositions were very similar (TR = 0.6-0.7 for f_{BEO} = 0.1-

0.50), with the exceptions of the two highest BEO content-blends; one of these resulted in a lower transfer ratio (TR = 0.5 for $f_{BEO} = 1$) and one showed a higher transfer ratio (TR = 1.9 for $f_{BEO} = 0.75$). The lack of a consistent trend between TR and composition indicates that transfer does not depend strongly on the blend composition, suggesting that neither component is transferred more easily to the solid substrates. This is understandable, since LB transfer occurs *via* wetting of the substrate with the water subphase at the three-phase contact line as the substrate is drawn through the air-water interface;[46] since the transfer process occurs before the thin layer of subphase dries, it is more strongly driven by the common affinity of the polymer components for the water surface than by the affinity of either component for the solid substrate.

Finally, in connection with the above discussion, the well-defined and size-variable domains in Figure 6 suggested to us the possible quantification of transferred blend compositions using image analysis of light and dark regions in Figure 6 (from TEM) together with height information from AFM. Unfortunately, such quantitative analysis was precluded by uncertainty in the relative amounts of PB and PS in the PB-rich and PS-rich domains, respectively. However, we point out that the essential finding in Figure 6 is that differences in blend composition effect systematic qualitative differences in the blend structure; this point is not diminished by the absence of a quantitative correlation between the blend composition and the images.

Conclusions

Concurrent self-assembly in various blends of PS-*b*-PEO and PB-*b*-PEO copolymers at the air-water interface generated hierarchical strand networks anchored *via* PEO blocks to the water surface with an internal phase-separation structure consisting of periodic domains of PS blocks surrounded and connected by a matrix of PB blocks. The resulting hierarchical structures were transferred within LB films to solid substrates, then imaged by a combination of TEM, with selective staining providing chemical identification of PS and PB phases, and tapping mode AFM, with topographical information providing determination of relative domain heights. The mutually supporting information from these complementary imaging methods allowed the unique hierarchical structures proposed in Figure 1 to be identified with confidence. For example, TEM images show that PB wets PS domains in the plane of the monolayer, while AFM images further show that PB wets PS domains in the orthogonal direction; both pieces of complementary information are consistent with reported critical surface tensions for the two polymers and support the proposed hierarchical structure. The self-assembled Langmuir films were also characterized *in situ* by compression isotherms at the water surface. This study presents a new concurrent self-assembly strategy for patterning hierarchical polymeric surface features based on the interplay of amphiphilic block copolymer aggregation at the air-water interface and polymer/polymer phase separation. The resulting multicomponent surface features with periodic hierarchical phase structure are fundamentally interesting as examples of simultaneous and synergistic processes of spontaneous structure formation on disparate length scales. They also point to a general and efficient strategy for manufacturing hierarchical polymeric surface features for applications ranging from electronics to biomaterials to medicine. Future work should explore multiscale

structural variability and surface patterning of these hierarchical features toward specific applications.

Supporting Information. Additional TEM images of LB films.

Acknowledgements. We are grateful to the Natural Sciences and Engineering Research Council of Canada, NSERC, for financial support. We also acknowledge Dr. Patrick Nahirney and Brent Gowen in the UVic EM lab (Department of Biology) for the continued use of their TEM and for assistance with sample preparation.

References

(1) Liu, Y.; Liu, B.; Nie, Z. *Nano Today* **2015**, *10*, 278-300.

(2) Klinger, D.; Wang, C. X.; Connal, L. A.; Audus, D. J.; Jang, S. G.; Kraemer, S.; Killops, K. L.; Fredrickson, G. H.; Kramer, E. J.; Hawker, C. J. *Angew. Chem. Int. Ed.* **2014**, *53*, 7018-7022.

(3) Baumgart, T.; Hess, S. T.; Webb, W. W. *Nature* **2003**, *425*, 821-824.

(4) Subramaniam, A. B.; Guidotti, G.; Manoharan, V. N.; Stone, H. A. *Nat. Mater.* **2013**, *12*, 128-133.

(5) Cheng, L.; Zhang, G.; Zhu, L.; Chen, D.; Jiang, M. *Angew. Chem. Int. Ed.* **2008**, *47*, 10171-10174.

(6) Rupar, P.; Chabanne, L.; Winnik, M.; Manners, I. *Science* **2012**, *337*, 559-562.

(7) Zhu, J.; Zhang, S.; Zhang, K.; Wang, X.; Mays, J. W.; Wooley, K. L.; Pochan, D. J. *Nat. Comm.* **2013**, *4*.

(8) Kang, Y.; Taton, T. A. *J. Am. Chem. Soc.* **2003**, *125*, 5650.

(9) Yusuf, H.; Kim, W.-G.; Lee, D. H.; Aloshyna, M.; Brolo, A. G.; Moffitt, M. G. *Langmuir* **2007**, *23*, 5251-5254.

(10) Yusuf, H.; Kim, W.-G.; Lee, D. H.; Guo, Y.; Moffitt, M. G. *Langmuir* **2007**, *23*, 868-878.

(11) Liu, Y.; Li, Y.; He, J.; Duelge, K. J.; Lu, Z.; Nie, Z. *J. Am. Chem. Soc.* **2014**, *136*, 2602-2610.

(12) Zhu, J.; Eisenberg, A.; Lennox, R. B. *J. Am. Chem. Soc.* **1991**, *113*, 5583-5588.

(13) Goncalves da Silva, A. M.; Filipe, E. J. M.; d'Oliveira, J. M. R.; Martinho, J. M. G. *Langmuir* **1996**, *12*, 6547-6553.

(14) Faure, M. C.; Bassereau, P.; Carignano, M.; Szleifer, I.; Gallot, Y.; Andelman, D. *Eur. Phys. J. B* **1998**, *3*, 365-375.

(15) Faure, M. C.; Bassereau, P.; Lee, L. T.; Menelle, A.; Lheveder, C. *Macromolecules* **1999**, *32*, 8538-8550.

(16) Cox, J. K.; Yu, K.; Constantine, B.; Eisenberg, A.; Lennox, R. B. P *Langmuir* **1999**, *15*, 7714 -7718.

(17) Devereaux , C. A.; Baker, S. M. *Macromolecules* **2002**, *35*, 1921 -1927.

(18) Cheyne, R. B.; Moffitt, M. G. *Langmuir* **2005**, *21*, 5453-5460.

(19) Cheyne, R. B.; Moffitt, M. G. *Langmuir* **2006**, *22*, 8387-8396.

(20) Lu, Q.; Bazuin, C. G. *Nano Lett.* **2005**, *5*, 1309-1314.

(21) Perepichka, I. I.; Badia, A.; Bazuin, C. G. *ACS Nano* **2010**, *4*, 6825-6835.

(22) Perepichka, I. I.; Lu, Q.; Badia, A.; Bazuin, C. G. *Langmuir* **2013**, *29*, 4502-4519.

(23) Li Destri, G.; Gasperini, A. A. M.; Konovalov, O. *Langmuir* **2015**, *31*, 8856-8864.

(24) Guennouni, Z.; Cousin, F.; Fauré, M.-C.; Perrin, P.; Limagne, D.; Konovalov, O.; Goldmann, M. *Langmuir* **2016**, *32*, 1971-1980.

(25) Yockell-Lelièvre, H.; Desbiens, J.; Ritcey, A. M. T *Langmuir* **2007**, *23*, 2843-2850.

(26) Yockell-Lelièvre, H. l. n.; Gingras, D.; Vallee, R.; Ritcey, A. M. *J. Phys. Chem. C* **2009**, *113*, 21293-21302.

(27) Cheyne, R. B.; Moffitt, M. G. *Langmuir* **2005**, *21*, 10297-10300.

(28) Cheyne, R. B.; Moffitt, M. G. *Macromolecules* **2007**, *40*, 2046-2057.

(29) Price, E. W.; Guo, Y.; Wang, C.-W.; Moffitt, M. G. *Langmuir* **2009**, *25*, 6398.

(30) Stefik, M.; Guldin, S.; Vignolini, S.; Wiesner, U.; Steiner, U. *Chem. Soc. Rev.* **2015**, *44*, 5076.

(31) Cabral, J.T.; Higgins, J.S. *Prog. Polym. Sci.* **2018**, *81*, 1.

(32) Kim, S. O.; Solak, H. H.; Stoykovich, M. P.; Ferrier, N. J.; de Pablo, J. J.;Nealey, P. F. *Nature* **2003**, *424*, 411.

(33) Stoykovich, M. P.; Muller, M.; Kim, S. O.; Solak, H. H.; Edwards, E. W.;de Pablo, J. J.; Nealey, P. F. *Science* **2005**, *308*, 1442.

(34) Li, W. H.; Muller, M. Prog. Polym. Sci. **2016**, *54*, 47.

(35) Boltau, M.; Walheim, S.; Mlynek, J.; Krausch, G.; Steiner, U. *Nature* **1998**, *391*, 877.

(36) Xue, L.J.; Zhang, J.L.; Han, Y.C. *Prog. Polym. Sci.* **2012**, *37*, 564.

(37) Harirchian-Saei, S.; Wang, M. C. P.; Gates, B. D.; Moffitt, M. G. *J. Colloid Interface Sci.* **2014**, *433*, 123.

(38) Sasaki, Y.; Aiba, N.; Hashimoto, H.; Kumaki, J. *Macromolecules* **2010**, *43*, 9077.

(39) Bernardini, C.; Cohen Stuart, M.; Stoyanov, S.; Arnaudov, L.; Leermakers, F. *Langmuir* **2012**, *28*, 5614.

(40) Sato, G.; Nishitsuji, S.; Kumaki, J. *J. Phys. Chem. B* **2013**, *117*, 9067.

(41) Kim, G.; Libera, M. *Macromolecules* **1998**, *31*, 2569.

(42) Erhardt, R. Bo1ker, A.; Zettl, H.; Kaya, H.; Pyckhout-Hintzen, W.; Krausch, G.; Abetz, V.; Müller, A. H. E. *Macromolecules* **2001**, *34*, 1069.

(43) McConnell, H. M. *Annu. Rev. Phys. Chem.* **1991**, *42*, 171.

(44) Turturrot, A; Gattiglia, E.; Vacca, P.; Viola, G. T. *Polymer* **1995**, *36*, 3987.

(45) Valentia, B.; Turturroa, A.; Losiob, S.; Falquib, F.; Costab, G.; Cavazzab, B.; Castellano, M. *Polymer* **2001**, *42*, 2427.

(46) Harirchian-Saei, S.; Wang, M. C. P.; Gates, B. G.; Moffitt, M. G. *Langmuir* **2010**, *26*, 5998.